Electronic Supplementary Material (ESI) for Soft Matter.

Supplementary Information

Fine tuning the structural colours of photonic nanosheet suspensions by polymer doping

Karin El Rifaii,[a] Henricus H. Wensink,[*a] Claire Goldmann,[a] Laurent Michot,[b] Jean-Christophe P. Gabriel[*c] and Patrick Davidson[a]

AFM and SEM characterization of the $H_3Sb_3P_2O_{14}$ nanosheets.

A sample for AFM and SEM was made by depositing a drop of solution of $H_3Sb_3P_2O_{14}$ at 1 g/L onto a clean Si wafer fragment (≈ 1 cm^2). The drop was left in contact for 5 min and then removed. Figure SI 1 presents a collage of adjacent images of the nanosheets recorded with a Hitachi S-4500 Scanning Electron Microscope (SEM) at a x1000 magnification and 25 kV acceleration voltage. Figure SI 2 displays an image of the same sample (different zone) obtained using a Digital Instrument Veeco Multimode Atomic Force Microscopy (AFM) equipped with Nanoscope® IIIa Scanning Probe Microscope controllers (with automated line flattening and no additional data treatment).

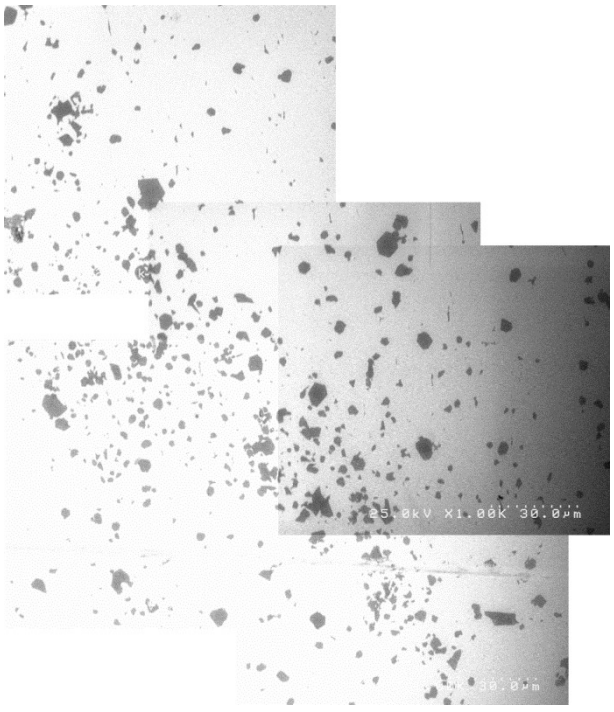

Figure SI 1. Typical scanning electron microscopy image of $H_3Sb_3P_2O_{14}$ nanosheets. The measurement of 340 particles provided their average diameter (1100 nm) and standard deviation (70%).

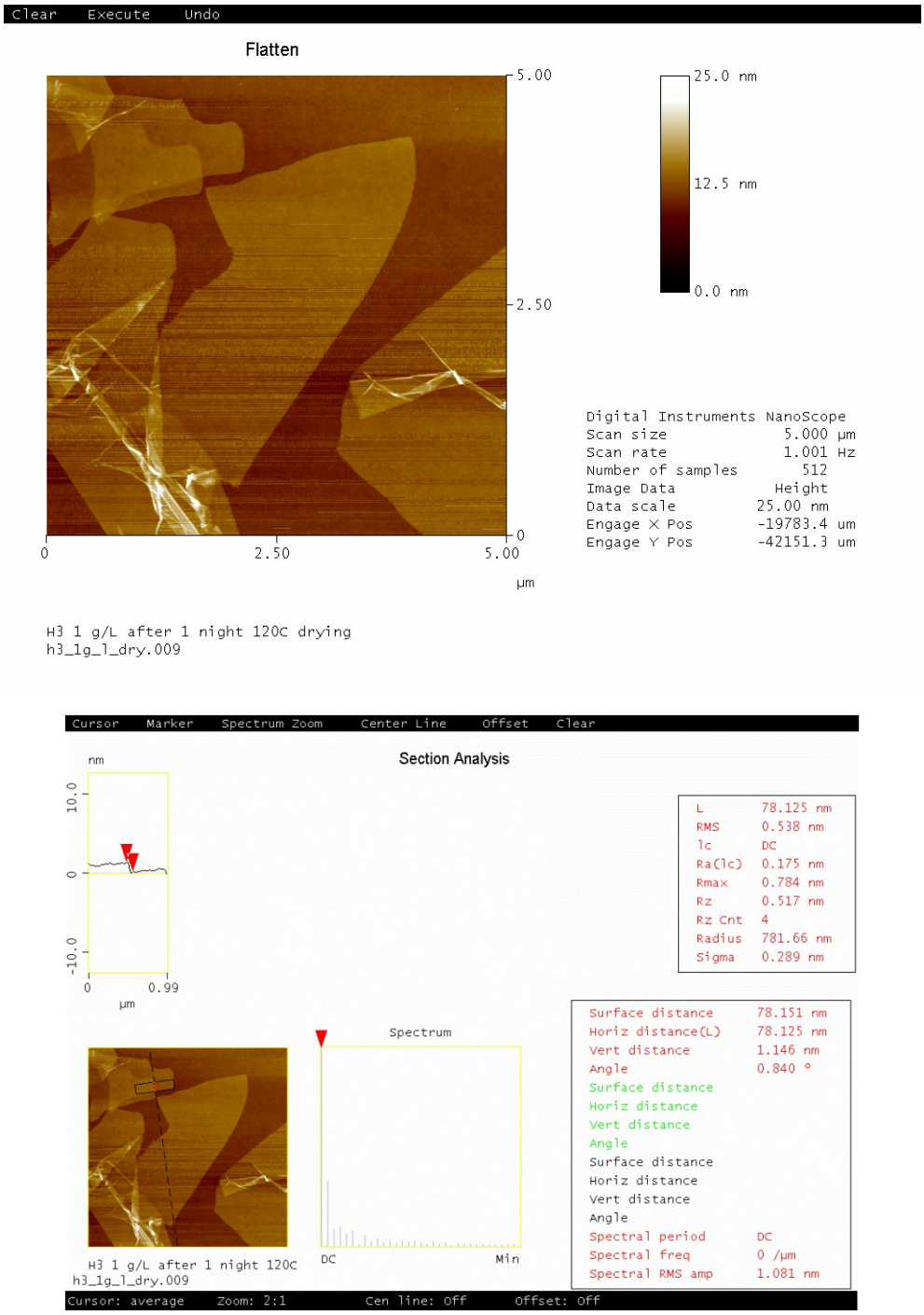

Figure SI 2. Top: Typical atomic force microscopy image of $H_3Sb_3P_2O_{14}$ nanosheets. Bottom: one example of vertical cut in the image showing that the nanosheet thickness is ≈1.1 nm.

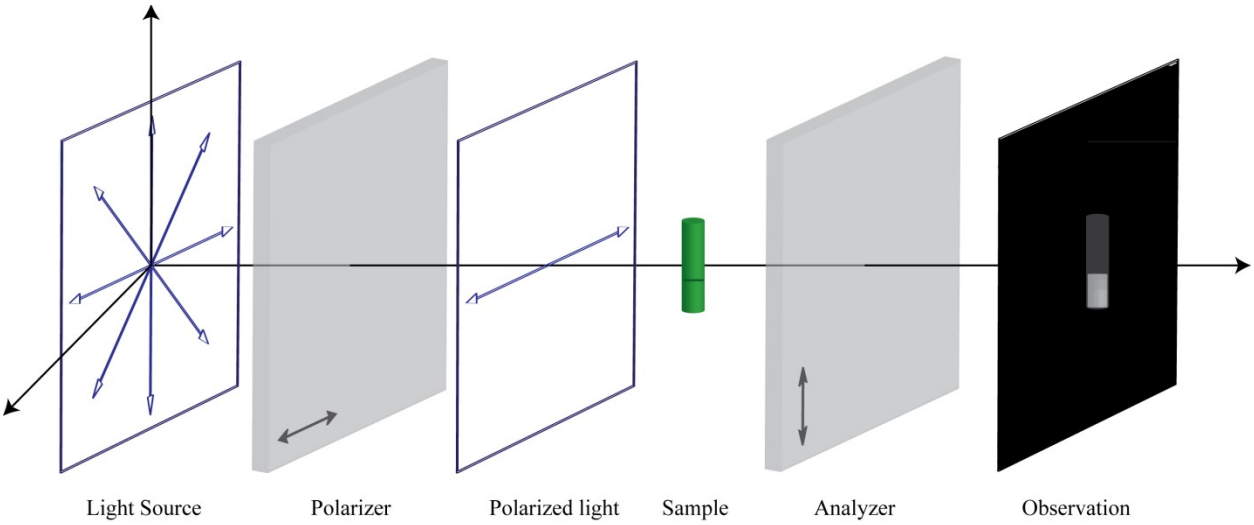

Figure SI 3. Left: Schematic representation of the "magic box" that allows for the observation of samples in polarized light. The blue double-headed arrows represent the polarization state of the light in the different parts of the device, the black double-headed arrows represent the polarizer and analyzer directions, and the green cylinder, placed between the polarizer and analyzer represents a biphasic sample, with a birefringent phase at the bottom and an isotropic phase at the top, as depicted at the observation level.

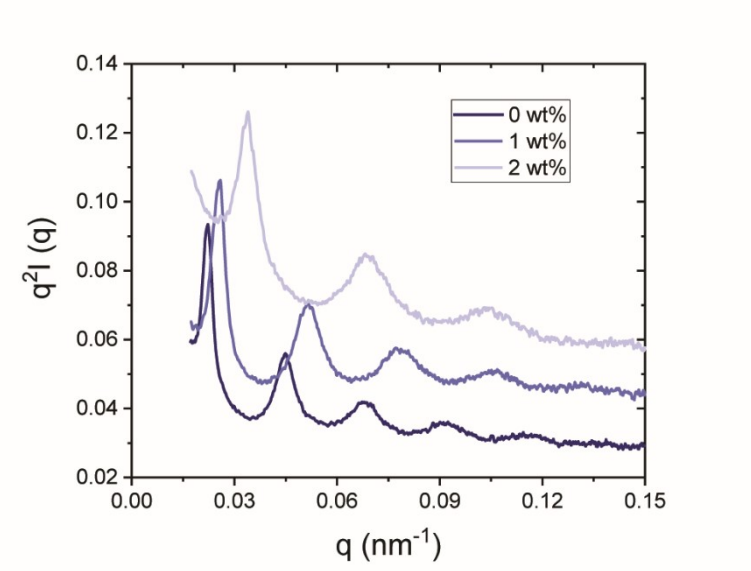

Figure SI 4. Curves of azimuthally-averaged scattered intensity in Kratky representation, $q^2.I(q)$ versus q, of three samples with same nanosheet weight fraction, C_{H3} = 0.16 wt%, but different PEO (100 kDa) weight fractions: 0, 1, and 2 wt%.

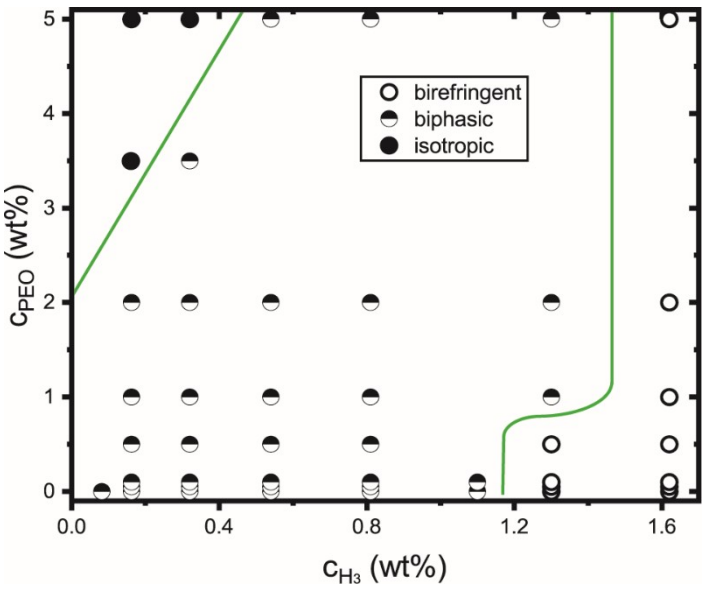

Figure SI 5. Experimental phase diagram of the PEO (100 kDa) /$H_3Sb_3P_2O_{14}$ colloidal suspensions. The green lines are guides to the eye indicating schematically the boundaries of the isotropic/birefringent nematic coexistence region.

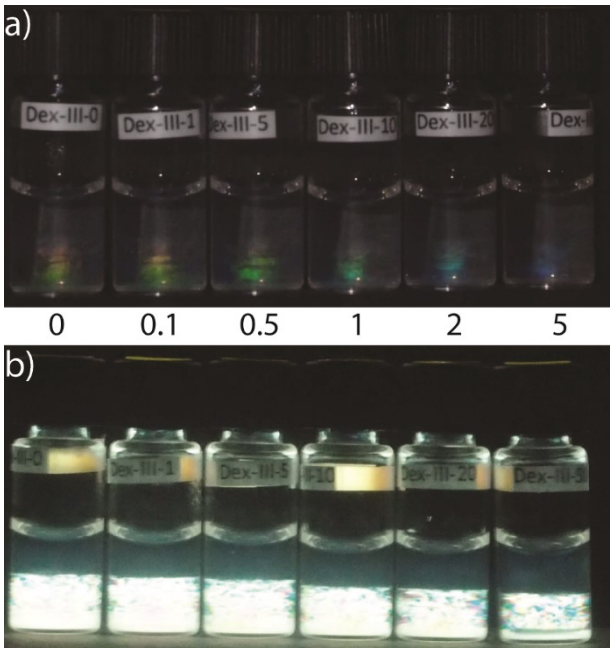

Figure SI 6. Photographs of a series of sample tubes, with constant C_{H3} = 0.54 wt% and dextran weight fraction increasing from left to right: C_{dex} = 0, 0.1, 0.5, 1, 2, and 5 wt%, observed a) in natural light: the structural color changes from red to blue due to dextran doping, and b) between crossed polarizers: the birefringent phase is barely destabilized.

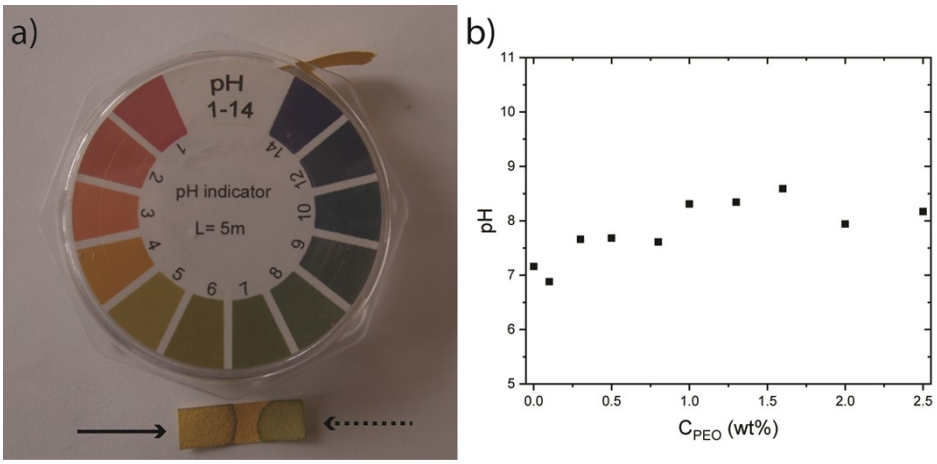

Figure SI 7.Lewis base character of PEO (100 kDa). a) Qualitative comparison of the pH (≈ 6) of a drop of pure water (solid arrow) with that (≈ 8) of a drop of PEO solution (25 g.L^{-1}, dashed arrow). The PEO solution clearly has a pH more basic than pure water. b) Dependence of pH on the PEO weight fraction, measured with a pH-meter.

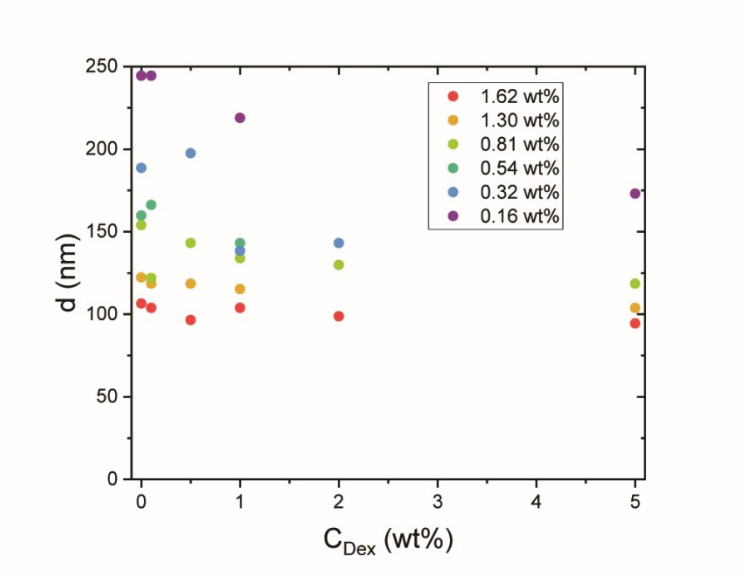

Figure SI 8.Dependence of the lamellar period on the dextran weight fraction for six series of samples with constant $H_3Sb_3P_2O_{14}$ weight fractions.

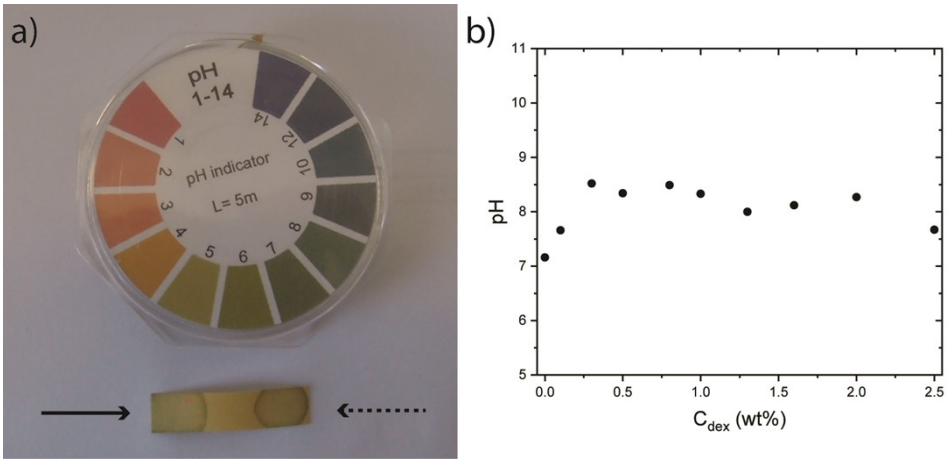

Figure SI 9.Lewis base character of dextran. a) Qualitative comparison of the pH (≈6) of a drop of pure water (solid arrow) with that (≈8) of a drop of dextran solution (25 g.L^{-1}, dashed arrow). The dextran solution clearly has a pH more basic than pure water. b) Dependence of pH on the dextran weight fraction, measured with a pH-meter.

Disjoining pressure from non-linear Poisson-Boltzmann theory:

The electrostatic potential ψ generated by two highly charged planar surfaces with equal charge density σ immersed in a monovalent 1:1 electrolyte follows from the non-linear Poisson-Boltzmann (PB) equation: (1,2)

$$\partial_z^2\psi(z) = \lambda_D^{-2} \sinh \psi(z) \qquad (20)$$

Where ψ has been implicitly normalized in units k_BT/e. The PB equation is subject to the boundary conditions $\partial_z\psi|_0 = \psi_m^{'} = 0$ at the lamellar mid-plane and $\partial_z\psi|_{\frac{d}{2}} = \psi_s^{'} = \frac{2}{l_{GC}}$ at the lamellar surface. Integration of the PB equation fulfilling the mid-plane boundary condition yields:

$$cosh\,\psi_s = cosh\,\psi_m + 2(\frac{\lambda_D}{l_{GC}})^2 \tag{21}$$

Similarly, implementing the boundary condition at the lamellar surface z = d/2 one finds:

$$\frac{d}{2\lambda_D} = \int_{\psi_m}^{\psi_s} \frac{d\psi}{\sqrt{2cosh\,\psi - 2cosh\,\psi_m}} \tag{22}$$

which may also be expressed in terms of elliptic integrals.(2) The boundary potentials $\psi_{m,s}$ for a given distance *d* are then easily resolved numerically from the coupled expressions above. By virtue of the contact theorem, the osmotic (disjoining) pressure between the lamellae is then obtained from the mid-plane potential:

$$\prod_{dis} = \frac{k_BT}{4\pi l_B \lambda_D^2}(\cosh\psi_m - 1) \tag{23}$$

A simple analytical form can be derived in the limit of very high surface charge density ($\lambda_D/\ell_{GC} >> 1$) and large intralamellar distance ($d/\lambda_D > 1$):

$$\prod_{dis} \approx \frac{8k_BT}{\pi l_B \lambda_D^2} exp\left(-\frac{d}{\lambda_D}\right) \tag{24}$$

which is compared against the numerical results in Figure SI 7 below.

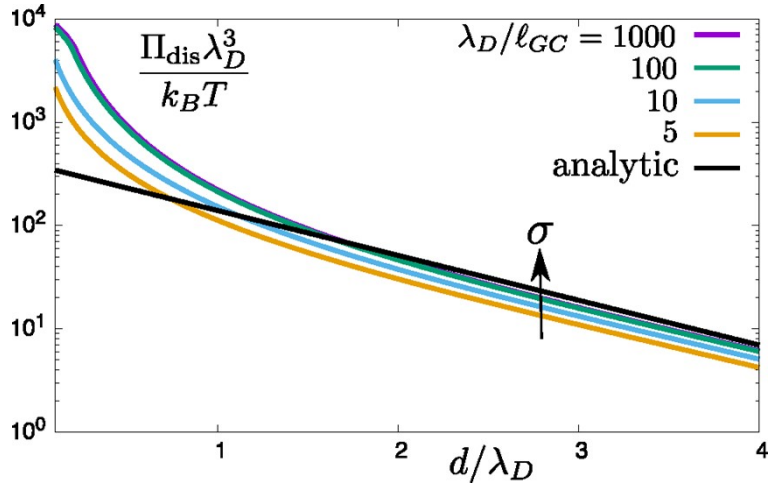

Figure SI 10: Disjoining pressure Π_{dis} between two uniformly charged lamellae at distance d from non-linear PB theory compared to the analytical approximation Eq. (24) for the intermediate regime.

1. Verwey EJW, Overbeek JTG, Nes K van. Theory of the Stability of Lyophobic Colloids: The Interaction of Sol Particles Having an Electric Double Layer. Elsevier Publishing Company; 1948. 228 p.

2. Andelman D. Electrostatic Properties of Membranes: The Poisson-Boltzmann Theory. In: Handbook of Biological Physics [Internet]. Elsevier; 1995 [cité 6 avr 2021]. p. 603-42. Disponible sur: https://linkinghub.elsevier.com/retrieve/pii/S1383812106800059